INTERNATIONAL JOURNAL OF REFRIGERATION 54 (2015) 190–203

Available online at www.sciencedirect.com

ScienceDirect

journal homepage: www.elsevier.com/locate/ijrefrig

Experimental investigation of a reversible heat pump/organic Rankine cycle unit designed to be coupled with a passive house to get a Net Zero Energy Building

Olivier Dumont[*], *Sylvain Quoilin* [1], *Vincent Lemort* [2]

Thermodynamics and Energetics Laboratory, Chemin des chevreuils, 7 B49, 4000 Liege, Belgium

ARTICLE INFO

Article history:
Received 12 September 2014
Received in revised form
4 March 2015
Accepted 5 March 2015
Available online 14 March 2015

Keywords:
Heat pump
Organic Rankine Cycle
Reversible
Experimentation
Net Zero Energy Building

ABSTRACT

This paper presents an innovative reversible Heat Pump/Organic Rankine Cycle (HP/ORC) experimental unit designed to be coupled to a Net Zero Energy Building (connected to a 120 m^2 thermal solar roof and a ground heat exchanger). The system can operate in three different modes: an ORC mode to produce electricity when a large amount of heat is collected by the solar roof, a direct heating mode using exclusively the solar roof, and a HP mode for space heating during cold weather conditions. This paper describes a comprehensive experimental campaign carried out on a prototype unit using a modified HVAC scroll compressor (4 kWe). From the results, the technical feasibility of the system is demonstrated. A cycle efficiency of 4.2% is achieved in ORC mode (with condensation and evaporation temperature respectively of 25 °C and 88 °C) and a COP of 3.1 is obtained in HP mode (with condensation and evaporation temperature respectively of 61 °C and 21 °C).

Etude expérimentale d'une pompe à chaleur réversible/d'un système à cycle organique de Rankine conçu pour une maison passive pour obtenir un bâtiment à consommation énergétique nulle

Mots clés : Pompe à chaleur ; Cycle organique de Rankine ; Réversible ; Expérimentation ; Bâtiment à consummation énergétique nulle

* *Corresponding author*. Tel.: +32 498/226404, +32 4 366 48 27.
E-mail addresses: Olivier.dumont@ulg.ac.be (O. Dumont), squoilin@ulg.ac.be (S. Quoilin), Vincent.Lemort@ulg.ac.be (V. Lemort).
[1] Tel.: +32 4 366 48 22.
[2] Tel.: +32 4 366 48 01.
http://dx.doi.org/10.1016/j.ijrefrig.2015.03.008
0140-7007/

Nomenclature

Variables

COP	Coefficient of performance [–]
cp	Specific heat [J (K kg)$^{-1}$]
g	Gravity [m s^{-2}]
h	Enthalpy [J (Kg)$^{-1}$]
H	Height [m]
$\dot{m}$	Mass flow [kg s^{-1}]
NPSH	Net Positive Suction Head [m]
P	Pressure [bar]
$\dot{Q}$	Heat transfer [W]
Res	Residual [W]
t	Temperature [°C]
$\dot{V}$	Volumetric flow [m^3 s^{-1}]
$\dot{W}$	Power [W]
X	Oil fraction [–]

Greek symbols

ρ	Density [kg m^{-3}]
ε	Effectiveness [–]
η	Efficiency [–]
ϕ	Filling factor [–]
φ	Kinetic energy factor [m^3 kg s^{-2}]
Δ	Difference [–]

Subscripts

amb	Ambient
cd	Condenser
cp	Compressor
el	Electrical
ev	Evaporator
ex	Exhaust
exp	Expander
Hp	Heat pump
hp	High pressure
is	Isentropic
lp	Low pressure
oil	Oil
ORC	Organic Rankine Cycle
pp	Pump
r	Refrigerant
sat	Saturation
sc	Sub-cooler
su	Supply
vol	Volumetric
th	Theoretical
tot	Total
w	Water

1. Introduction

By 2020, greenhouse gases emissions must be reduced by 20% as compared to the levels of 1990, according to European objectives (20–20–20 objectives) (European Commission, 2012). This goal will be achieved both through an increase in the proportion of renewable energy from 9% to 20%, and an increase in energy system efficiency of 20%. Households account for 27% of the final energy consumption (European Commission, 2011) and therefore have the potential to contribute significantly to the targeted reduction in emissions.

Various technologies and concepts are being investigated, developed and implemented in the building sector. In this particular project, five different concepts are combined: Net Zero Energy Buildings (NZEB), heat pumps (HP), solar energy, micro-combined heat and power generation (μCHP) and the Organic Rankine Cycle (ORC).

Net Zero Energy Buildings (Jagemar et al., 2010; Kurnitski et al., 2014) are expected to gain a significant importance: by 2019, all new buildings should present a total renewable energy production higher than their primary energy consumption (European commission, 2010). This concept has already been successfully implemented using solar thermal and photovoltaic collector technology (Saitoh and Fujino, 2001). An alternative is the integration of a reversible HP/ORC, which constitutes a promising solution for NZEBs.

The use of water-to-water heat pumps is an established technology that allows the production of heat efficiently in various applications (Hepbasli and Yalinci, 2009). It is estimated that in the European Union, a reduction of 54% of CO_2 emissions could be achieved with the introduction of heat pumps into the building sector (Bettgenhäuser et al., 2013). The prototype unit presented in this paper is very similar to a classical water-to-water heat pump in terms of components and costs (see Section 3.3).

There is a necessity to increase the share of renewable resources in the primary energy balance, both for environmental reasons and energy security (European Commission, 2012). The International Energy Agency (IEA) projections involve, among others, a 16% coverage of the needs of low temperature heat by solar heating (International Energy Agency, 2012). However, thermal collectors are characterized by the mismatch between heat supply and demand, i.e., during summer months, the heat demand is at its lowest at a time when heat production through the solar collectors is the highest. This leads to the necessity to either undersize the solar collectors (leading to low solar factors), or to collect a large amount of unused heat. Thus, using any excess heat to produce electricity constitutes an interesting option, given an appropriate conversion technology such as the proposed HP/ORC unit.

The idea of using solar powered Rankine system for domestic applications has been investigated for several years (Wolpert and Riffat, 1995). Although PV panels produce electricity with a higher efficiency (≈12%–20%) than current low temperature (<100 °C) ORC systems (≈12%) (Twomey et al., 2013), some authors have shown that low temperature ORCs could reach a potential efficiency of up to 20% by using an

advanced components and zeotropic mixtures (Bao et al., 2011). Furthermore, the proposed ORC system allows for Combined Heat and Power production (CHP) and can shift its electrical production in time with a storage system. This is a non-negligible advantage in terms of flexibility and load shifting on future electric grids.

Few publications report successful experimental investigations on the use of solar energy to produce electricity at a domestic scale with Rankine cycles. In 1997, a Rankine cycle was used to recover solar energy at low temperature (165 °C) and produced around 2.24 kWe of electricity (Almanza and Lentz, 1998). Later, in 2001, a radial flow turbine was used in a hybrid gas burner/solar system to produce 1.5 kWe (Oliveira et al., 2002). In 2002, a hybrid ORC system combining diesel and solar energy was tested successfully with scroll expanders (Kane et al., 2003). Following that, an experimental investigation of a small-scale solar ORC heat engine for distributed power was carried out in 2009 (Orosz et al., 2009). In 2010, a rolling-piston expander was used to produce up to 1.73 kW using heat energy from flat plate and evacuated tube collectors (Wang et al., 2010). Recently, a 2 kWe Rankine cycle with 2D tracking parabolic trough collector for CHP has been tested (Bouvier, 2013) and a two-stage micro solar ORC with two scroll expanders working in series was investigated (Georges et al., 2013) and tested (Dickes et al., 2014). Several proof-of-concept implementations of such units have been successfully tested, however, the technology has not yet reached commercial maturity.

Combined heat and power generation can be implemented to produce electricity with a small environmental footprint in some applications. CHP has the potential to provide more than 30% of the Europe's electricity while not reducing the continent's heat independency (European Commission, 2011). A potential advantage of distributed power generation is that it can avoid the electricity transportation losses characteristic of large, centralized power networks (Oliveira et al., 2002). Furthermore, the thermal energy exhausted form large-scale plants often cannot be further utilized economically. Lower capacity CHP plants constitute an interesting alternative to the traditional centralized power plants (Oudkerk et al., 2011).

In this work, a micro CHP plant is theoretically investigated. The plant design chosen for investigation uses flat plate solar collectors combined with a gas burner, as described by Facao et al. (2008). Recent works on small-scale solar cogeneration ORCs using scroll expanders present encouraging estimations of the dynamic performance (Twomey et al., 2013; Ziviani et al., 2014). An experimental 3 kWe ORC designed for CHP has been shown to be interesting economically with an overall cost of 3000$ (Malavolta et al., 2010). Multiple publications also suggest that scroll expander is particularly appropriate expansion technology for micro-CHP application (<10 kWe) (Qiu et al., 2011; Quoilin, 2011).

In conclusion, the elements integrated into this project (NZEB, solar energy, ORC, HP, CHP) promise to be massively deployed in the future. The heat pump is used to efficiently produce thermal energy for a house in winter. The solar energy generated by the roof can be used to produce electricity through an ORC system and to fulfil directly the heat requirements of the house when appropriate (CHP possibility). Finally, this system coupled to a passive house is a promising way to achieve a Net Zero Energy Building at a manageable economic cost.

This paper contains four parts. The first part is a description of the reversible HP/ORC unit with its three different operating modes. Then, the experimental setup is presented detailing all of the components and sensors. In the third part, results from the experimental campaign are described and discussed. Finally, interesting prospects and conclusions are formulated in the fourth section.

2. Description of the HP/ORC system and its operating modes

A micro-scale Organic Rankine Cycle contains very similar technology to that of a heat pump; refrigerants, compressor, evaporator, condenser, regenerator. After having proved the feasibility of reversing a scroll compressor to run as a scroll expander, the idea of using one single unit that could work in both modes (heat pump and ORC) is a logical next step. The reversible HP/ORC unit investigated in this paper is originally a water-to-water heat pump connected to a 138.8 m^2 solar roof (Innogie, 2013) and to a horizontal ground heat exchanger (Fig. 1).

By adding a pump to the classic heat pump design and reversing the rotation of the scroll compressor (Saitoh et al., 2007; Lemort et al., 2009; Orosz et al., 2009; Quoilin, 2011; Lu et al., 2012), it is possible to run it as an ORC to generate electricity (Innogie, 2013; Dumont et al., 2014). The goal is to provide electricity in summer months thanks to the ORC mode and heating from the heat pump in winter months. In addition to the ORC and HP modes, a third operating mode is defined; when the solar source is used directly for space heating or domestic hot water production. The flowchart from Fig. 2 presents a simplified scheme describing the selection between the three operating modes. It should be noted that this figure outlines a preliminary control strategy, not an optimal control system based on weather forecast, storage temperature, ground temperature and heat demand.

The technology of reversible HP/ORC unit coupled to a building has been investigated for the first time in 2011 (Schimpf et al., 2011). In this study, the authors developed a simulation tool to evaluate the economical benefits of such a concept using only a small thermal roof (12 m^2) and a vertical ground heat exchanger. Later, in 2013, the concept of a passive house with a large solar absorber (138.8 m^2) coupled with a horizontal ground heat exchanger (300 m long) has been

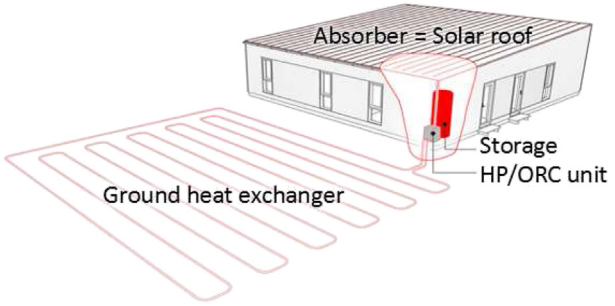

Fig. 1 – The reversible HP/ORC unit integrated in a residential building (Innogie, 2014).

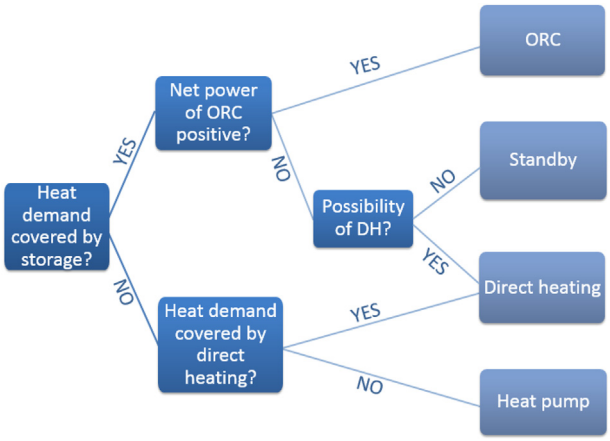

Fig. 2 – Flowchart to select the operating mode.

patented (Innogie, 2013). Finally, an optimization of the size of the system has been completed, and promising results have been announced. The optimized system model indicates a net electrical production of 2609 kWh/year while also meeting the space heating demands (Dumont et al., 2014).

2.1. *Organic Rankine Cycle mode (ORC)*

This mode converts the thermal energy absorbed by the solar collector on the roof into electricity. The ORC mode (Fig. 3) is run when the meteorological conditions are sufficient to get a positive net electrical production and the heat demand of the house can be covered by thermal energy in the storage tank (Fig. 2). The pump increases the pressure of the working fluid which then passes through to an evaporator, where the fluid is vaporized using the thermal energy from the solar roof. Following that, the working fluid flows into the expander (modified compressor) where electricity is produced. Thermal energy is then transferred from the working fluid in the ground heat exchanger, and the fluid is condensed. In addition to these components, a liquid receiver (tank) is used to handle the variation of the refrigerant charge and a four-way valve allows switching between the inlet and outlet of the compressor (see Section 4.1).

2.2. *Direct heating mode (DH)*

In this mode, heat absorbed by the solar roof is directed to the storage through an intermediate heat exchanger (Fig. 4). The direct heating mode is used to heat the storage at times when the storage temperature is not sufficient to cover the heat demand of the house, as long as there is enough incident solar energy to raise the supply temperature in the storage to a sufficient level.

2.3. *Heat pump mode (HP)*

When direct heating is not sufficient to fulfil the heat demand of the house, the heat pump mode is activated to increase the storage temperature (Fig. 5). First, the compressor increases the pressure and temperature of the working fluid to release its heat in the storage through the condenser. The refrigerant then flows into the expansion valve and is further evaporated at a low temperature thanks to the thermal energy from the roof.

3. Experimental setup

3.1. *Layout*

In order to verify the promising simulation results described previously by the authors (Dumont et al., 2014), an experimental study is performed on the HP/ORC prototype with refrigerant R134a (annex: Fig. 17 of Dumont (2014)). A scheme of the test rig is outlined in Fig. 6 with the main elements shown; compressor, evaporator, condenser, pump and valves. The refrigerant loop (dark blue) also includes a liquid receiver for charge variations and a subcooler used to provide a sufficient degree of subcooling at the inlet of the pump. This loop also includes a four-way valve that allows for switching between ORC and HP modes and a bypass valve that is necessary to start the expander in ORC mode. The evaporator is supplied by a water loop (red) connected to an electrical boiler (150 kW). The condenser is cooled by tap water (light blue) to simulate

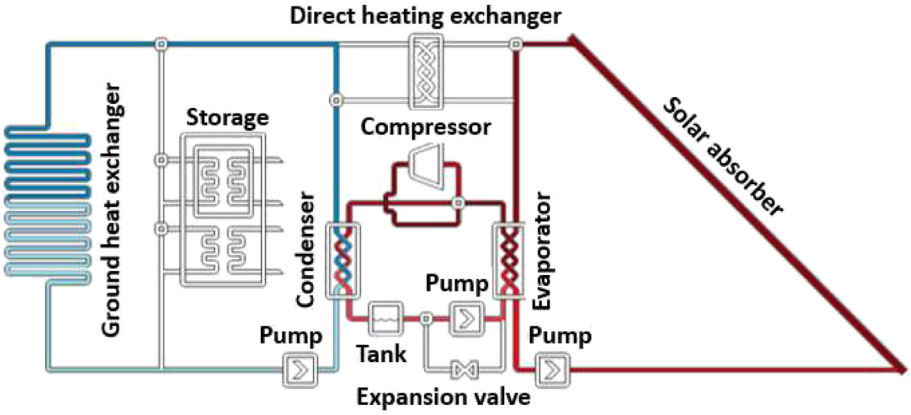

Fig. 3 – Simplified scheme of the unit (ORC mode).

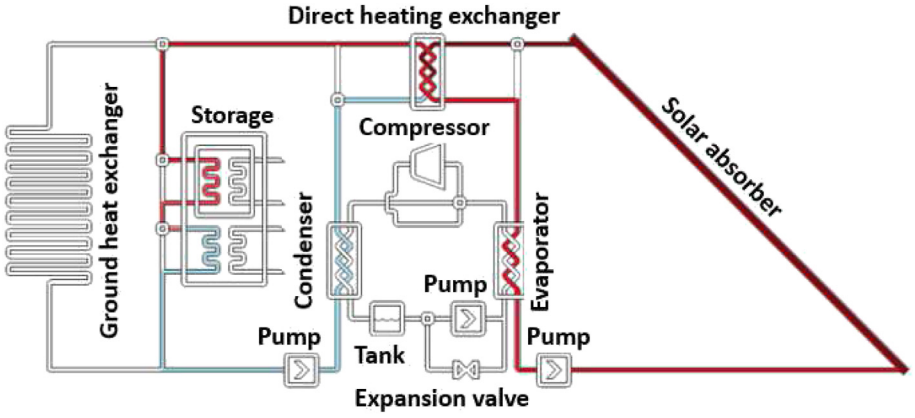

Fig. 4 – Simplified scheme of the unit (direct heating mode).

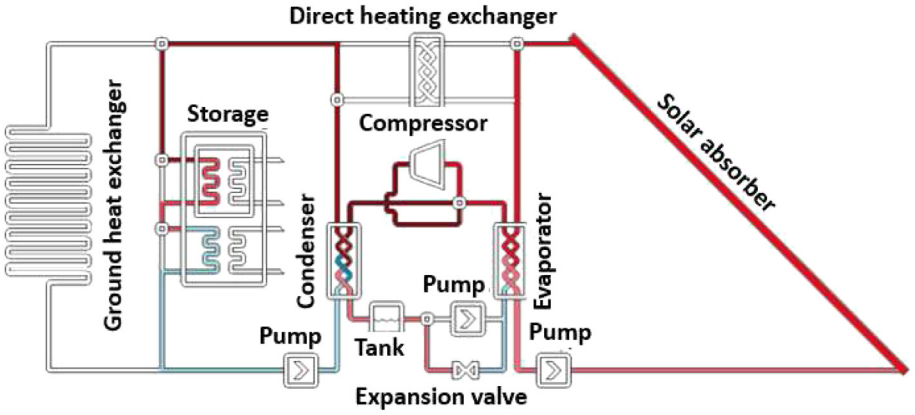

Fig. 5 – Simplified scheme of the unit (HP mode).

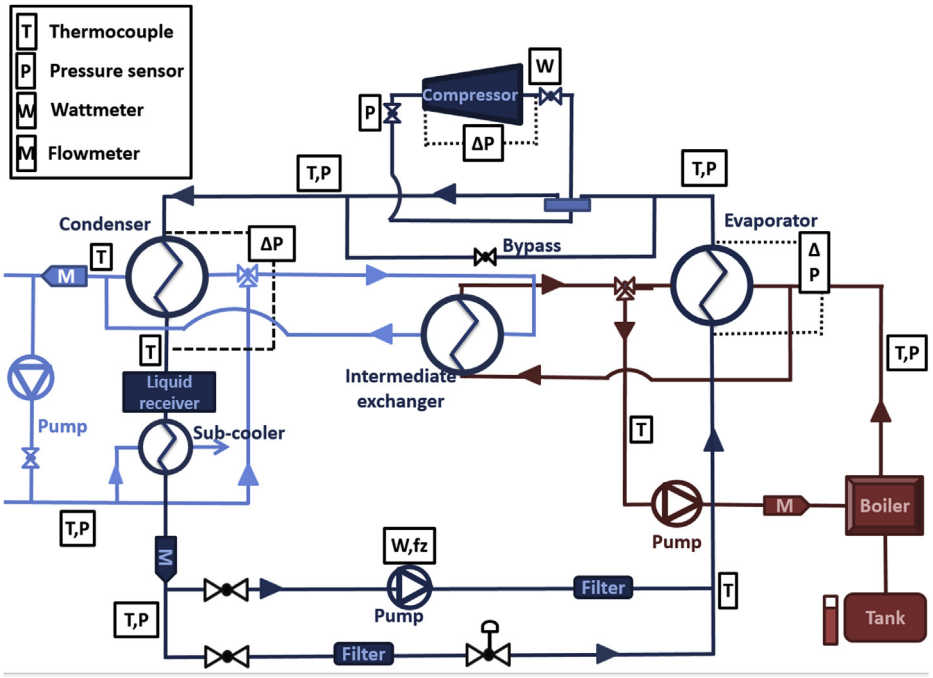

Fig. 6 – Detailed scheme of the experimental setup (dark blue = refrigerant loop, red = heating loop and light blue = cooling loop). (For interpretation of the references to colour in this figure legend, the reader is referred to the web version of this article).

the cold water flow in the storage or the ground heat exchanger, depending on the mode of operation.

3.2. Components

The design step and technological choices were based on a simulation model and presented by the authors (Dumont et al., 2014). The selected components will therefore only be briefly presented in this paper.

The same scroll machine is used as both the expander (ORC) and the compressor (HP). Scroll machines are well proven for the compression of refrigerants in small systems around the targeted heating capacity. In expander mode, this technology is also particularly suitable for the low targeted electrical output (<10 kW) (Qiu et al., 2011; Quoilin, 2011). Compressor selection was performed by comparing the net electrical production (ORC production minus heat pump consumption) over a whole year (Dumont et al., 2014). The optimum sizing of the scroll machine results in a trade-off between winter and summer conditions. The selection of an expander (or compressor) with an overly small displacement will constrain the maximum electrical production, and hence prevent the maximum usage of the heat generated in summer. A too large displacement leads to low electrical production because the scroll machine must then work at part load most of the time. The compressor is connected to the grid (50 Hz) and therefore runs at a constant speed (neglecting the slip of the induction motor). A phase inverter allows switching from compressor mode to expander mode. To the authors' knowledge, it is the first time that an off-the-shelf HVAC scroll compressor has been used as a compressor and as an expander in the same application. The compressor has been modified following the methodology proposed by Quoilin (2011). These modifications include the opening of the casing, the removal of the check valve and the addition of a spring below the floating seal.

Plate-type heat exchangers are used for the evaporator and condenser (Table 1). They are selected for their compactness, efficiency and low cost. The pump is a volumetric plunger-type pump. The pump's rotational speed is controlled by an inverter (Table 1). An electronic expansion valve is chosen for its controllability compared to traditional expansion valves (Table 1).

3.3. Sensors

This section summarizes the data acquisition (DAQ) system together with the technical data of the sensors. The pressure and flow sensors are described in Table 2. A Coriolis flowmeter is used to measure the refrigerant mass flow rate with high accuracy. The cold loop and hot loop water volumetric flow rates are measured manually with water counters. All temperatures are measured by T-type thermocouples. Their measuring range is between −200 °C and 350 °C, with a maximum error of ± 0.5 K. Watt-meters are used to measure the electrical power consumption of the pump and compressor.

4. Experimental results

4.1. Measurements validation

Experimental campaigns are often subject to measurements issues such as sensor malfunction, operator misuse or data acquisition failure. Therefore, it is of primary importance to crosscheck the experimental data for consistency using all possible redundancies in the measured data, performing heat balances on all components and checking that the measured data is self-consistent. The following verifications have been performed:

- Global residual (Eq. (1), (annex: Figs. 18 and 19 of Dumont (2014))

$$Res_{global} = \dot{Q}_{ev,w} + \dot{W}_{cp/exp,el} - \dot{Q}_{cd,w} - \dot{Q}_{sc,r} + (\dot{W}_{pp,el}) \quad (1)$$

Table 1 – Technical data of the compressor, evaporator, condenser, pump and expansion valve.

Component	Parameter	Value
Compressor	Displacement (compressor mode) [cm^3]	82.6
	Built-in volume ratio [–]	2.8
	Max pressure [bar]	32
	Motor power at max current [kW]	4
Evaporator	Exchange area [m^2]	4.08
	Max. pressure [bar]	32
	Max temperature [°C]	225
Condenser	Exchange area [m^2]	3.12
	Max. pressure [bar]	32
	Max temperature [°C]	225
Pump	Maximum flow [l/min]	15.1 (at 1725 RPM)
	Max. pressure [bar]	206
	Max temperature [°C]	121
	Motor [kW]	1.5
Expansion valve	Flow direction	Unidirectional
	Max. pressure [bar]	45
	Max temperature [°C]	100
	Nominal thermal heat at the condenser [kW]	13

Table 2 – Sensors technical data (FS = full scale).

Sensors	Location	Range	Accuracy [%FS]
Pressure	Condenser in and Condenser out [bar]	[0:25]	0.5
	Evaporator out [bar]	[0:40]	0.5
	Cold water and hot water [bar]	[0:6]	0.5
	Scroll suction port (compressor) [bar]	[0:20]	0.05
	Scroll ex (compressor) [bar]	[0:40]	0.3
	Difference condenser [bar]	[0:0.3]	0.5
	Difference evaporator [bar]	[0:0.15]	0.5
	Difference scroll [bar]	[0:20]	1
Flow	Refrigerant [kg/s]	[0:0.3]	0.2
	Cold water [m^3/h]	[0:3]	1
	Hot water [m^3/h]	[0:10]	1
Wattmeter	Pump [W]	[−2000:2000]	0.5
	Compressor/expander [W]	[−6000:6000]	0.5

- Heat balance on the condenser and evaporator (Eq. (2), annex: Figs. 22 and 23 of Dumont (2014))

$$\dot{m}_r(h_{r,su} - h_{r,ex}) + \dot{m}_{oil}\cdot cp_{oil}\cdot(t_{r,su} - t_{r,ex}) = \dot{m}_w\cdot cp_w(t_{w,ex} - t_{w,su}) \quad (2)$$

- Residual on the compressor and expander (Eq. (3), annex: Figs. 26 and 27 of Dumont (2014))

$$Res_{cp} = \left|\dot{W}_{cp,el} - \dot{m}_r(h_{r,ex} - h_{r,su}) - \dot{m}_{oil}\cdot cp_{oil}\cdot(t_{r,ex} - t_{r,su}) - \dot{Q}_{cp,amb}\right| \quad (3)$$

The verifications show that the residual of each balance is lower than the uncertainty propagation error for the different components for almost all the points. The few exceptions encountered can be explained by the solubility of oil and ambient losses not having been taken into account. Measurements are presented in two separate tables (Dumont, 2014).

Table 3 – Minimum and maximum values of the main parameters in HP mode.

Parameter	Nomenclature	Minimum	Maximum
Condenser thermal power [kW]	$\dot{Q}_{cd,r}$	9	17
Evaporation pressure [bar]	P_{ev}	3	6.5
Condensation pressure [bar]	P_{cd}	6	20.5
Mass flow rate [kg/s]	$\dot{m}_{tot}$	0.049	0.113
Compressor power consumption [kW]	$\dot{W}_{cp,el}$	1.87	4.3
Coefficient of performance [−]	COP	2.7	7.1
Compressor isentropic efficiency [%]	$\varepsilon_{cp,is}$	69	79
Compressor volumetric efficiency [%]	$\varepsilon_{cp,vol}$	95	115

4.2. Heat pump performance

4.2.1. Range of operating conditions and achieved performance

Table 3 presents the variation range of the main operating conditions observed in heat pump mode for the 31 stabilized measurement points (Dumont, 2014). Performance is assessed in terms of coefficient of performance (COP), volumetric efficiency and isentropic efficiency, defined according to Eqs. (4)–(6). m_{tot} is defined as the sum of refrigerant and oil mass flow rates. Table 3 also shows the condenser thermal power on the refrigerant side ($\dot{Q}_{cd,r}$), the electrical power consumption of the compressor ($\dot{W}_{cp,el}$), the evaporation pressure (P_{ev}) and condensation pressure (P_{cd}).

$$\varepsilon_{cp,is} = \frac{\dot{m}_{tot}(h_{cp,ex,is} - h_{cp,su})}{\dot{W}_{cp,el}} \quad (4)$$

$$\varepsilon_{cp,vol} = \frac{\dot{V}_{cp,su}}{\dot{V}_{cp,th}} \quad (5)$$

$$COP = \frac{\dot{Q}_{cd,r}}{\dot{W}_{cp,el}} \quad (6)$$

4.2.2. Comparison with theoretical nominal point

In a previous publication by the authors (Dumont et al., 2014), the design and the sizing of the test bench has been performed using validated semi-empirical models of each component. A nominal steady-state operating point was defined for both the HP and ORC modes. It is therefore of interest to compare the experimental data with the predicted nominal conditions. This comparison is presented in Table 4 with key performance data and in Fig. 7 with the comparison of the theoretical and measured temperature–entropy diagrams. The different steps of the process are observed in Fig. 7: expansion valve exhaust and evaporator supply (1), evaporator exhaust and four-way valve (low pressure lp) supply (2), four-way valve (Lp) exhaust and compressor supply (3), compressor exhaust and four-way valve (high pressure hp) supply (4), four-way valve (Hp) exhaust and condenser supply (5), condenser exhaust and sub-cooler supply (6), sub-cooler exhaust and expansion valve supply (7).

Table 4 – Comparison of the results between experiments and theory (HP).

Parameter	Nomenclature	Theoretical nominal	Experimentation
Condenser thermal power [kW]	$\dot{Q}_{cd}$	13	11
Evaporation pressure [bar]	P_{ev}	5	4
Condensation pressure [bar]	P_{cd}	17	15.9
Mass flow rate [kg/s]	$\dot{m}_r$	0.1	0.066
Compressor power consumption [kW]	$\dot{W}_{cp,el}$	3.09	3.5
Coefficient of performance [–]	COP	4.2	3.14
Compressor isentropic efficiency [%]	$\varepsilon_{cp,is}$	69	66
Compressor volumetric efficiency [%]	$\varepsilon_{cp,vol}$	91	95

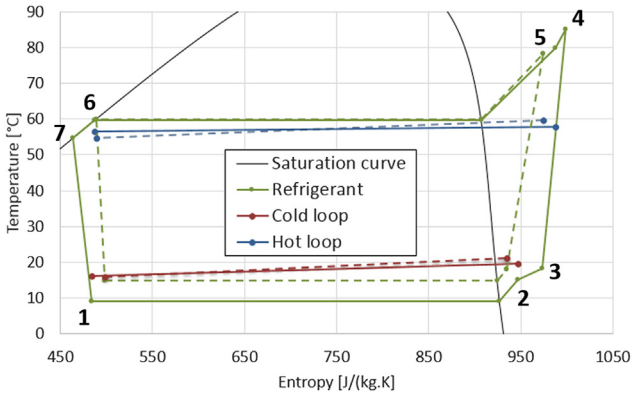

Fig. 7 – T–S diagram for the HP mode (Dashed lines = theoretical cycle, plain lines = actual cycle).

The performance of the experimental system is slightly lower than theoretical predictions for electrical power consumption and COP. This is explained by the following:

- An unexpectedly high pressure drop through the four-way valve (up to 1 bar) upstream from the compressor inlet (see Section 4.2.5).
- The nominal point was defined with a subcooling of 2 K. However, in this unit, an additional subcooling is necessary to ensure accurate measurement in the Coriolis flowmeter (where two-phase flow and vapor bubbles are not acceptable). In Fig. 7, a 6 K sub-cooling is observed at the inlet of the expansion valve, 4 K greater than in the theoretical model.
- Fig. 7 also shows that non-negligible heat transfer occurs between the high and low pressure sides in the four-way valve, i.e. the refrigerant is heated before entering the compressor and the refrigerant is cooled down at the exhaust of the compressor. This heat exchange reaches a magnitude of up to 200 W depending on the data points.
- Finally, a higher degree of superheat was present in the experiment than was assumed for the model (6 K compared to the assumed value of 3 K). This extra superheating was necessary to avoid unsteady conditions at the compressor inlet (annex: Fig. 28 of Dumont (2014)).

4.2.3. *Global performance*

As shown in Fig. 8, and in agreement with heat pump theory, the COP decreases with an increase in the temperature lift requirement (Eq. (7)). The measured COP values range between 3.1 and 3.8 around the nominal temperature lift of 45 K.

$$lift = \left|t_{ev,sat} - t_{cd,sat}\right| \tag{7}$$

4.2.4. *Compressor performance*

Fig. 9 presents the isentropic and volumetric efficiencies of the compressor versus the pressure ratio. It should be noted that the evaluation of the oil fraction in the test rig's scroll volume remains an unknown since there is no easy way to measure it, however, considering the amount of oil introduced in the system, the fraction is estimated to be lower than 10%. Error bars indicate its influence on the measured performance with a maximum representative 10% oil mass fraction (Eqs. (8)–(11)).

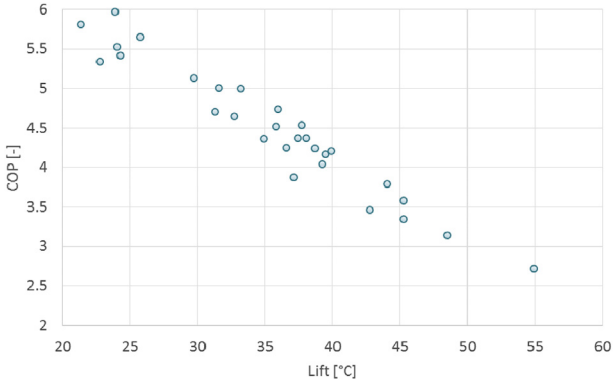

Fig. 8 – Coefficient of Performance versus lift.

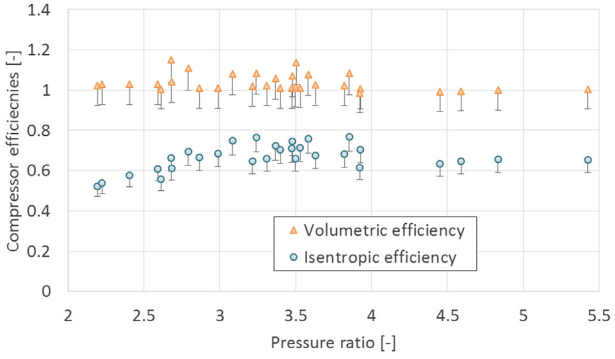

Fig. 9 – Evolution of the volumetric and isentropic efficiencies with the pressure ratio.

$$\dot{m}_r = (1 - X)\dot{m}_{tot} \quad (8)$$

$$\dot{m}_{oil} = X \cdot \dot{m}_{tot} \quad (9)$$

$$\varepsilon_{cp,vol,oil} = \frac{\dot{V}_{cp,r,su} + \dot{V}_{cp,su,oil}}{\dot{V}_{cp,th}} \quad (10)$$

$$\varepsilon_{cp,is,oil} = \frac{\dot{m}_r\left(h_{cp,ex,is} - h_{cp,su}\right) + \dot{V}_{oil}\left(P_{cp,ex} - P_{cp,su}\right)}{\dot{W}_{cp,el}} \quad (11)$$

Further investigation will be undertaken in future to determine the oil mass fraction accurately. The uncertainty error propagation was found to be negligible compared to the uncertainty on the oil mass fraction. Fig. 9 shows that compressor volumetric efficiency is consistently close to unity, with some relatively high values greater than 1.1. These higher values can most likely be explained by the effect of the oil mass fraction in the scroll volume. Isentropic efficiency conforms to expectations (less than 5% error with the manufacturer data) and the maximum is reached at nominal volume ratio.

4.2.5. *Heat exchangers*

For clarity, only minimum and maximum values of the pinch-point temperature in the heat exchangers are presented in Table 5. The pressure drops (Fig. 10) and pinch-points are found to be small for both the evaporator and the condenser. Pressure drops are proportional to kinetic energy, presented as a function of the kinetic energy factor (Eq. (12)). As the flow is always turbulent, the pressure drop is expected to be linearly proportional to the kinetic energy factor if the friction factor is considered constant.

$$\varphi = \frac{\dot{m}_r^2}{\rho} \quad (12)$$

4.3. *Organic Rankine Cycle mode*

4.3.1. *Range of operating conditions and achieved performance*

Table 6 presents the range of the 39 stabilized measurement points in ORC mode (Dumont, 2014). The performance is assessed in terms of the overall efficiency, the isentropic efficiency and the filling factor (equivalent of the volumetric efficiency for an expander) evaluated through Eqs. (10), (13) and (14).

$$\eta_{global} = \frac{\dot{W}_{exp,el} - \dot{W}_{pp,el}}{\dot{Q}_{ev,r}} \quad (13)$$

$$\varepsilon_{exp,is} = \frac{\dot{W}_{exp,el}}{\dot{m}_{tot}\left(h_{exp,su} - h_{exp,ex,is}\right)} \quad (14)$$

Table 5 – Exchanger performance in HP mode.

Exchanger	Evaporator	Condenser
Pressure drop [bar]	[0.048:0.133]	[0.043:0.062]
Pinch-point [K]	[0.2:7.6]	[2.1:5.1]

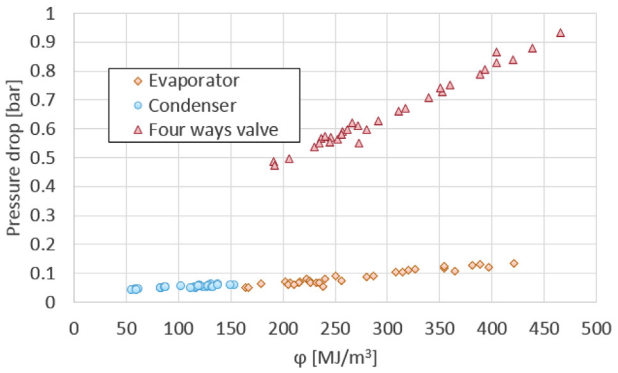

Fig. 10 – Pressure drops (HP mode).

4.3.2. *Comparison with theoretical nominal point*

In the same manner as for the heat pump measurements, Table 7 and Fig. 11 present a comparison between the experiment and the theoretical nominal operating point. The following flow stages are presented in Fig. 11: Subcooler exhaust and pump supply (1), pump exhaust and evaporator supply (2), evaporator exhaust and four-way valve supply (High pressure Hp) (3), four way valve exhaust (Hp) and expander supply (4), expander exhaust and four way valve (Lp) supply (5), four way (Lp) exhaust and condenser supply (6) and, condenser exhaust and subcooler supply (7).

The performance is lower than expected by the theoretical model in terms of electrical power generation and efficiency. This is explained by:

- A low expander isentropic efficiency (see section 4.3.4). In Fig. 11, a higher entropy expansion is indeed observed during the experiment (see section 4.3.4).
- In Fig. 11, a significant pressure drop (up to 3.6 bar) is observed in the four-way valve at the exhaust of the expander (see Section 4.2.5).
- An higher than expected subcooling is required to avoid any pump cavitation (Section 4.3.5). In Fig. 11, a 10 K subcooling is observed at the exhaust of the sub-cooler.

Table 6 – Minimum and maximum values of the main operating conditions and performance in ORC mode.

Parameter	Nomenclature	Minimum	Maximum
Evaporator thermal power [kW]	$\dot{Q}_{ev}$	30	65
Evaporation pressure [bar]	P_{ev}	16	32
Condensation pressure [bar]	P_{cd}	5.4	10.2
Mass flow rate [kg/s]	$\dot{m}_r$	0.124	0.294
Expander electrical production [kW]	$\dot{W}_{exp,el}$	0.125	3.696
Global efficiency [%]	η_{global}	0	5.3
Expander isentropic efficiency [%]	$\varepsilon_{exp,is}$	10	63
Expander filling factor [–]	ϕ_{exp}	1	1.1

Table 7 – Comparison of the results between experiments and theory (ORC).

Parameter	Nomenclature	Theoretical nominal	Experimentation
Evaporator thermal power [kW]	$\dot{Q}_{ev}$	62	62
Evaporation pressure [bar]	P_{ev}	33	32
Condensation pressure [bar]	P_{cd}	7	10.3
Mass flow rate [kg/s]	$\dot{m}_r$	0.3	0.266
Expander electrical production [kW]	$\dot{W}_{exp,el}$	5.9	3.7
Global efficiency [%]	η_{global}	7.5	4.2
Expander isentropic efficiency [%]	$\epsilon_{exp,is}$	68	58
Expander filling factor [–]	ϕ_{exp}	1.019	1.02

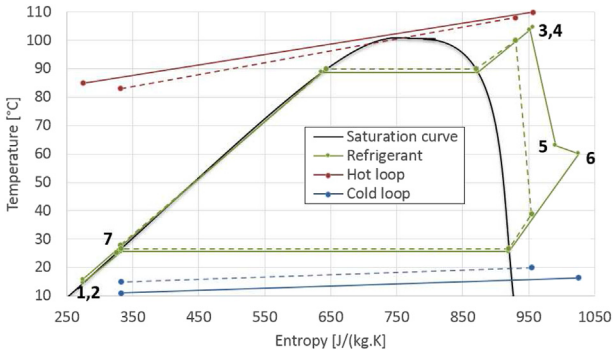

Fig. 11 – T-s diagram for the ORC mode (comparison between experiments and theory). Dashed lines = Theory, plain line = experiment.

4.3.3. *Overall efficiency*

Fig. 12 shows the overall efficiency (Eq. (13)) versus temperature lift (Eq. (7)). The overall efficiency of the ORC and the power production increases with an increase in temperature lift as expected, until the efficiency reaches a maximum value of 5.2%. It should be noted that the optimal efficiency is reached at part load (i.e. with low mass flow) because it avoids the occurrence of an excessive pressure drop in the four-way valve.

The pressure drop in the low pressure side of the four-way valve (see Section 4.2.5) is found to reduce the overall efficiency. If this pressure drop did not occur, the expander exhaust pressure would be significantly lower, leading to a greater pressure difference across the expander (and thus to a higher electrical production). The global efficiency of the unit is simulated without the four-way valve pressure drop, and is presented in Fig. 12. A higher impact from the pressure drop could be expected at high temperature lift conditions (i.e. high flow and thus high pressure drop) but this is balanced by the decrease of the isentropic efficiency of the expander when increasing the pressure ratio (i.e. high pressure ratio and therefore high over-expansion losses).

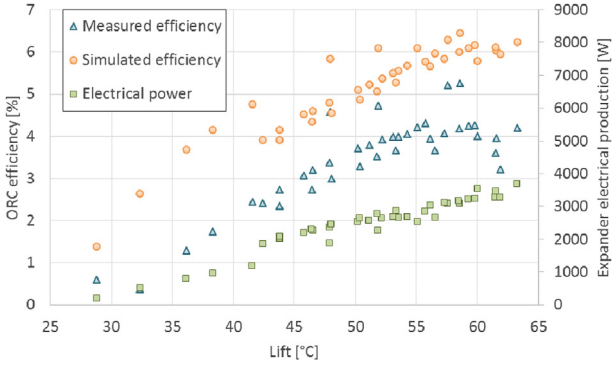

Fig. 12 – ORC efficiency versus lift Measured global efficiency and simulated global efficiency evaluated by deleting the pressure drop on the four way valve and expander electrical production.

4.3.4. *Expander performance*

Fig. 13 presents the filling factor (as defined in Eq. (5)) and the isentropic efficiency (Eq. (14)) of the expander. The influence of the unknown oil mass fraction is greater than the measurement uncertainty propagation and is represented through error bars indicating the impact of a 10% oil mass fraction (similar to the compressor – Eqs. (10) and (11)).

The filling factor is close to unity for each point except when working at low pressure ratio (values below 2.3). This could be explained by unloading phenomenon between the two scrolls leading to larger flank leakages. The isentropic efficiency is increasing with the pressure ratio up to 0.63. This efficiency is slightly lower than the efficiency of other scroll machines reported in literature (Aoun and Clodic, 2008; Lemort et al., 2009; Quoilin, 2011; Zanelli and Favrat, 1994; Yanagisawa et al., 1990; Manzagol et al., 2002) but this could be explained by the adaptations made to the scroll unit in order to work both in compressor and in expander, and by the relatively high oil fraction. The use of an expander with a dedicated expansion geometry (not a modified compressor)

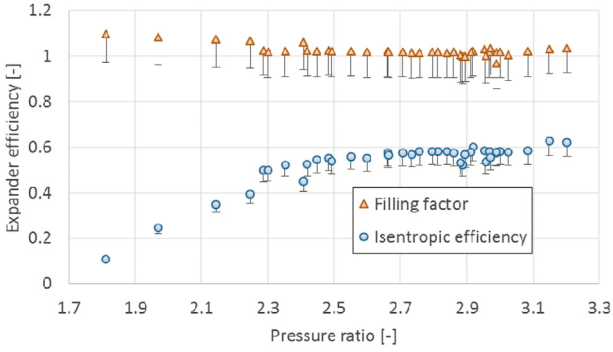

Fig. 13 – Evolution of the expander filling factor and isentropic efficiency with the pressure ratio.

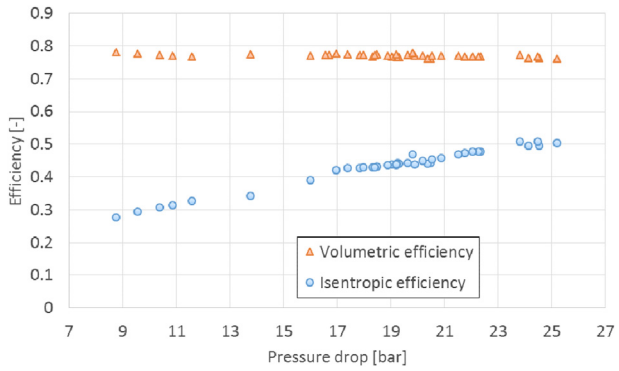

Fig. 14 – Pump efficiency.

and a dedicated motor is expected to increase the efficiency above what is observed in this experiment.

4.3.5. *Pump performance*

The refrigerant pump has been tested over a large range of pressure differences [8.7 bar–25.2 bar] (Fig. 14). The volumetric efficiency (Eq. (5)) is found to be nearly constant and presents a slight decrease at high pressure difference, which could be explained by an increase of internal leakages. The isentropic efficiency (Eq. (4)) increases with increasing pressure difference up to 50%. The main explanation is that the electrical motor efficiency is low when working at part load conditions (i.e. low pressure ratios). This isentropic efficiency is rather high for this type of applications (small power and low working fluid viscosity) compared to literature (Quoilin, 2014). The pump electrical efficiency could be significantly increased with a smaller motor (i.e. 1 kW instead of 1.5 kW).

The volumetric efficiency versus NPSH, defined by Eq. (15), is presented in Fig. 15. This figure shows that this pump requires a relatively high NPSH (around 10 m) corresponding to a minimum necessary subcooling of around 10 K. This is necessary to avoid cavitation. One explanation for the observed spread of the measurement points is because the refrigerant level H above the pump is not measured, and so is assumed to be constant at 1 m.

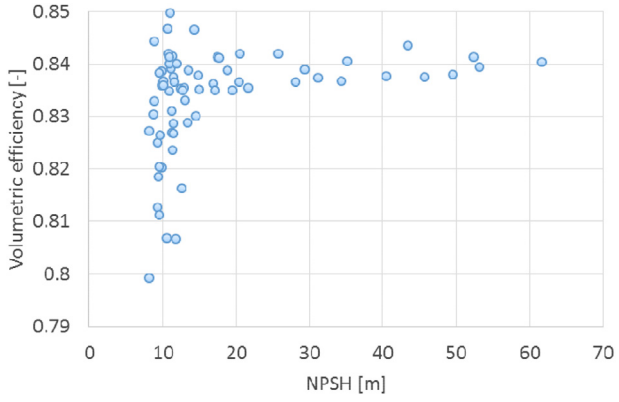

Fig. 15 – Pump volumetric efficiency.

Table 8 – Range of measured heat exchanger performance metrics in ORC mode.

Exchanger	Evaporator	Condenser
Pressure drop range [bar]	[0.023:0.09]	[0.151:0.46]
Pinch-point range [K]	[0.4:8.8]	[0:13]

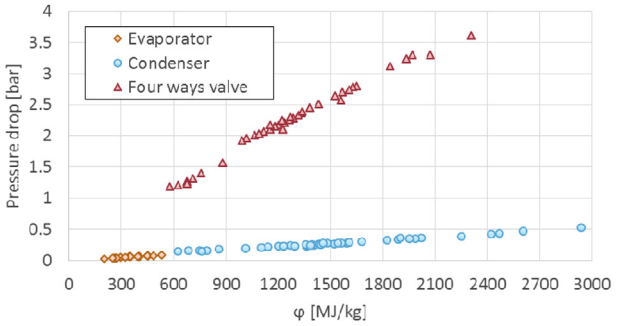

Fig. 16 – Pressure drops (ORC).

$$NPSH = H + 10^5 \left(\frac{p_{cd,ex} - p_{pp,sat}}{\rho g} \right) \quad (15)$$

4.3.6. *Heat exchangers*

Similar to the heat pump operating mode, only the minimum and the maximum values of the pinch-point temperature in the exchangers are presented in Table 8 for clarity. Globally, the observed pinch-points and pressure drops (Fig. 16) are relatively small, indicating that the evaporator and the condenser are correctly sized for this application. The results presented show that the condenser has a non-negligible pressure drop of above 0.5 bar at high flow rates. It should be noted that the pressure drop sensor is installed to include a 30 cm long section of pipe in the test set up, adding to the measured pressure drop.

5. Conclusion

Former studies in literature (Schimpf et al., 2011, Quoilin, 2013) have assessed the theoretical environmental and economic potential of this reversible HP/ORC unit. This paper presents an experimental test setup, and the main results of experiments carried out in the Thermodynamics Laboratory in Liège.

The results from the experimental setup presented prove the feasibility of the HP/ORC concept, and indicate encouraging performance for the system. The heat pump provided a COP of 3.1 at the nominal point (evaporation temperature of 21 °C and condensation temperature of 61 °C). In ORC mode, a maximum thermal efficiency of 4.2% was measured at an evaporation temperature of 88 °C and condensation temperature of 25 °C with a gross power output of 3.7 kW.

Some weaknesses are identified in the experimental setup which explain its lower performance compared to theoretical

predictions: the pressure drop and heat transfer occurring in the four-way valve, the lower than normal expander efficiency, the high NPSH of the pump and the lack of insulation on the test unit. The four way valve pressure drop can be reduced by using a valve with a larger cross-sectional area, or by removing this component altogether and using another system architecture. The expander efficiency could be improved by using a purpose-built expander geometry and a motor instead of an off-the-shelf compressor. Another pump design with a lower NPSH requirement could help to reduce the required sub-cooling.

Several improvements to future experimental setups can be recommended from these conclusions. First, the significant influence of the oil fraction on the results indicates that it is necessary to develop the experimental analysis in order to determine it precisely. These measurements can be used to calibrate semi-empirical models so as to predict the performance with a wide range of inputs. Finally, dynamic simulations of the experimental unit coupled to the house envelope, the storage, the solar roof and the ground heat exchanger could provide useful additional information, such as an economic comparison with other technologies, comparison of different climates and house envelope, comparison of different storage sizes, and the potential benefits of more developed control strategies, among others.

Annex

Fig. 17 – Picture of the reversible HP/ORC unit.

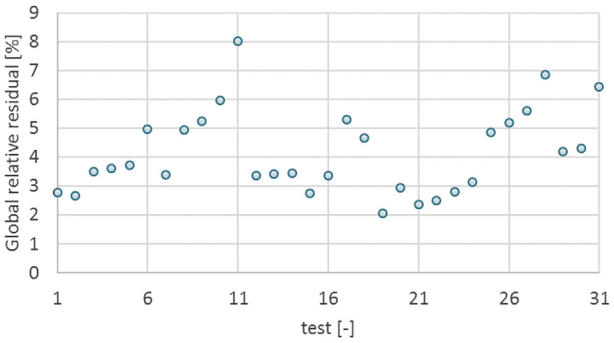

Fig. 18 – Global relative residual (heat pump).2

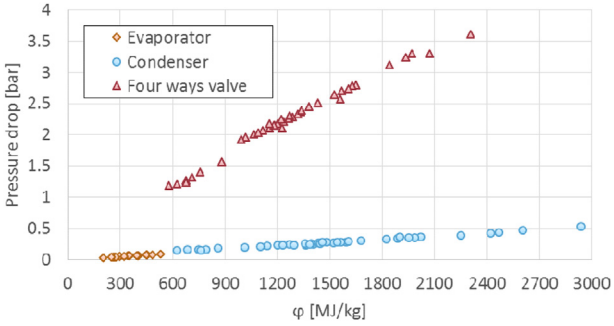

Fig. 19 – Global relative residual (ORC).3

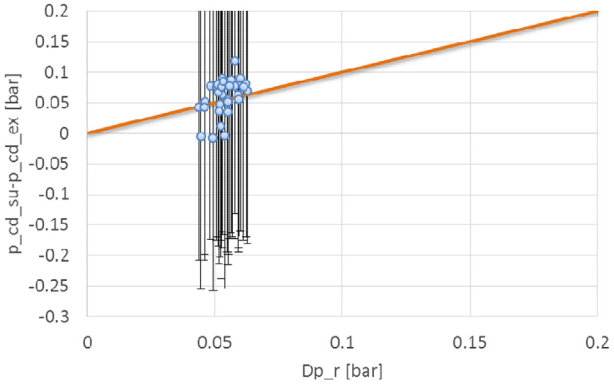

Fig. 20 – Cross-checking of pressure sensor of the condenser (Heat pump).4

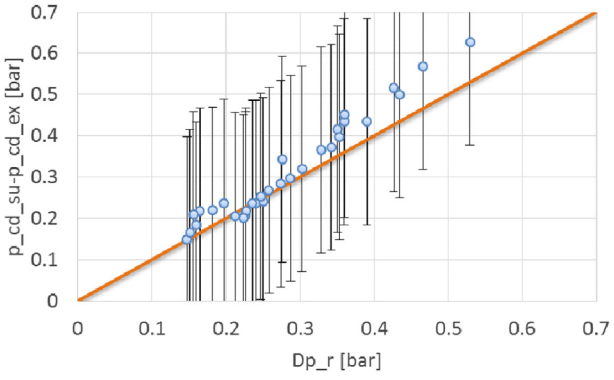

Fig. 21 – Cross-checking of pressure sensor of the condenser (ORC).5

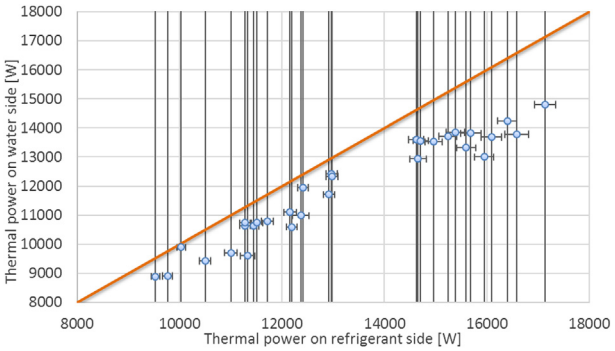

Fig. 22 – Heat balance on the condenser (heat pump).6

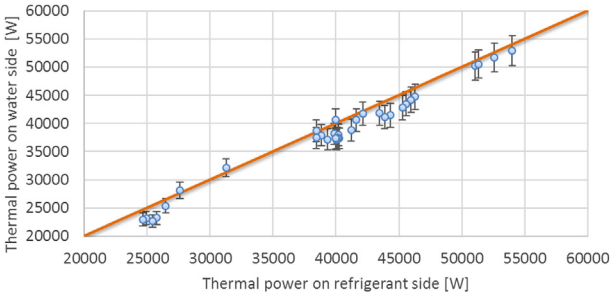

Fig. 23 – Heat balance on the condenser (ORC).7

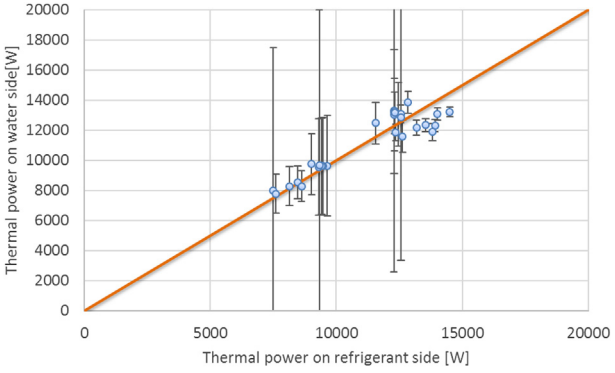

Fig. 24 – Evaporator heat balance (heat pump mode).8

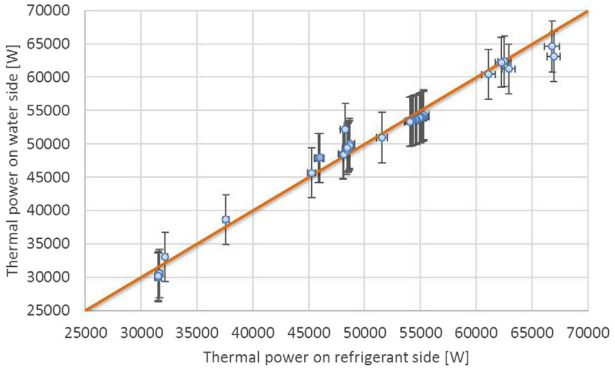

Fig. 25 – Evaporator heat balance (ORC generation mode).9

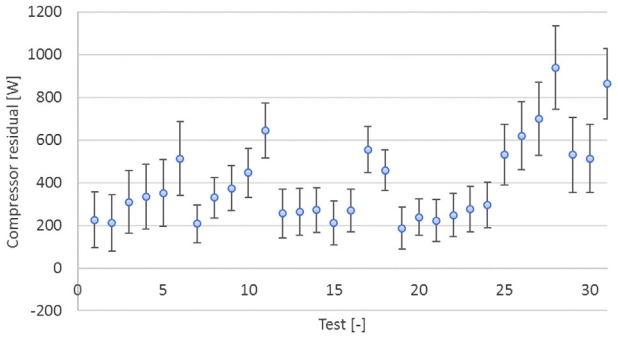

Fig. 26 – Compressor residual.10

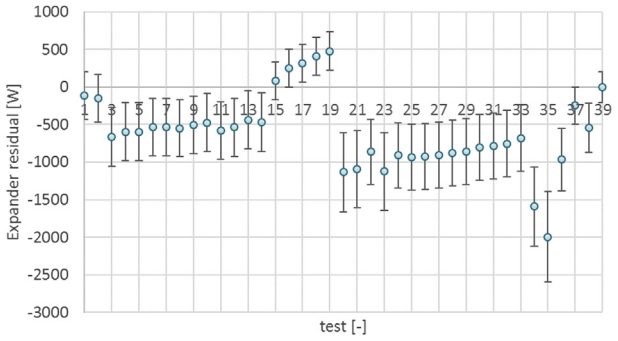

Fig. 27 – Expander residual.1

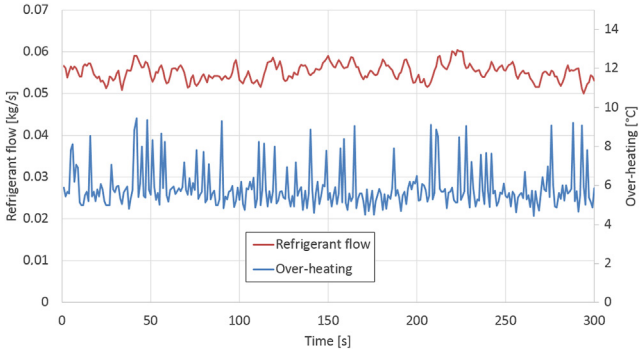

Fig. 28 – Oscillations of the flow due to the electronic expansion valve. This is observed when the set-point of over-heating is low.2

REFERENCES

Almanza, R., Lentz, A., 1998. Electricity production at low power by direct steam generation with parabolic troughs collectors. Sol. Energy 64, 115–120.

Aoun, B., Clodic, D., 2008. Theoretical and experimental study of an oil-free scroll vapor expander. In: International Compressor Engineering Conference, 1925.

Bao, J., Zhao, L., Zhang, W.Z., 2011. A novel auto-cascade low-temperature solar rankine cycle for power generation. Sol. Energy 85, 2710–2719.

Bettgenhäuser, K., Offermann, M., Boermans, T., Bosquet, M., Grözinger, J., von Manteuffel, B., Surmeli, N., 2013. Heat Pump Implementation Scenarios until 2030: an Analysis of the Technology's Potential in the Building Sector of Austria, Belgium, Germany, Spain, France, Italy, Sweden and the United Kingdom. Ecofys. Report, Project number: BUIDE12080.

Bouvier, J.L., 2013. Prototype d'un micro-cogénérateur à nergie solaire: MICOSOL. In: Proceedings of Journées Micro-cogénération CNAM Paris 2013.
Dickes, R., Dumont, O., Declaye, S., Quoilin, S., Bell, I., Lemort, V., 2014. Experimental investigation of an ORC system for a micro-solar power plant. In: Proceedings of International Compressor Engineering Conference at Purdue 2014.
Dumont, O., 2014. Annexes – Experimental Investigation of a Reversible Heat Pump/Organic Rankine Cycle Unit Designed to be Coupled with a Passive House (Net Zero Energy Building). http://hdl.handle.net/2268/171478.
Dumont, O., Quoilin, S., Lemort, V., 2014. Design, modelling and experimentation of a reversible HP/ORC prototype. In: Proceedings of the 11th International Energy Agency Heat Pump Conference.
European Comission, 2010. Directive 2010/31/CE of the European Parliament and of the Council of 19 May 2010.
European Comission, 2011. Market Observatory for Energy.
European Commission, 2012. Communication from the Comission to the European Parliament, the Council, the European Economic and Social Comittee and the Committee of the Regions, Brussel.
Facao, J., Palmero-Marrero, A., Oliveira, A.C., 2008. Analysis of a solar assisted micro-cogeneration ORC system. Int. J. Low-Carbon Tech. 3 (4), 254–264.
Georges, E., Declaye, S., Dumont, O., Quoilin, S., Lemort, V., 2013. Design of a small-scale Organic Rankine Cycle engine used in a solar power plant. Int. J. Low Carbon Tech. 8 (1), 34–41.
Hepbasli, A., Yalinci, Y., 2009. A Review of Heat Pump Water Systems, IRESR, vol. 13, pp. 1211–1229.
Innogie ApS, 2013. Thermal solar absorber system generating heat and electricity, United States Patent Application Publication, US 2013/025778 A1.
Innogie ApS, 2014. Innogie website, http://www.innogie.dk, Consulted 12th of January 2014.
International Energy Agency, 2012. Technology Roadmap – Solar Heating and Cooling.
Jagemar, L., Schmidt, M., Allard, F., Heiselberg, P., et Kurnitski, J., 2011 May 2011. Towards NZEB – some example of national requirements and roadmaps. Rehva J. 14–17.
Kane, M., Larrain, D., Favrat, D., Allani, Y., 2003. Small hybrid solar system. Energy 28, 1427–1443.
Kurnitski, J., Corgnati, S., Tiziana, B., Derjanecz, A., Litiu, A., 2014 March 2014. NZEB definitions in Europe. Rehva J. 6–9.
Lemort, V., Quoilin, S., Cuevas, C., Lebrun, J., 2009. Testing and modeling a scroll expander integrated into an Organic Rankine Cycle. Appl. Therm. Eng. 29 (14–15), 3094–3102.
Lu, Y.J., Wang, L.W., Tian, G.H., Roskilly, A.P., 2012. Study on a small scale solar powered organic rankine cycle utilizing scroll expander. In: 4th International Conference Applied Energy.
Malavolta, M., Beyene, A., Venturini, M., 2010. Experimental implementation of a micro-scale ORC-based CHP energy system for domestic applications. In: Proceedings of the ASME 2010 International Mechanical Engineering Congress & Exposition.
Manzagol, J., Harboulle, P., Claudet, G., Baguer, G., 2002. Cryogenic scroll expander for claude cycle with cooling power of 10 to 100 Watts at 4.2 K. AIP Conf. Proc. 613 (1), 267.
Oliveira, A.C., Alfonso, C., Matos, J., Riffat, S., Nguyen, M., Doherty, P., 2002. A combined heat and power system for buildings driven by solar energy and gas. Appl. Therm. Eng. 22, 587–593.
Orosz, M., Mueller, A., Quoilin, S., Hemond, H., 2009. Small scale solar ORC system for distributed power. In: Solar World Congress 2009.
Oudkerk, J.F., Quoilin, S., Lemort, V., 2011. Evaluation of an ORC-based micro-CHP system involving a hermetic scroll expander. In: Proceedings of the ORC 2011 Conference.
Qiu, G., Liu, H., Riffat, S., 2011. Expanders for micro-CHP systems with Organic Rankine Cycle. Appl. Therm. Eng. 31, 3301–3307.
Quoilin, S., Dumont, O., Lemort, V., 2013. Design, modeling and performance optimisation of a reversible HP-ORC prototype. In: 2nd International Seminar on ORC Power Systems, Rotterdam.
Quoilin, S., 2011. Sustainable Energy Conversion through the Use of Organic Rankine Cycles for Waste Heat Recovery and Solar Applications (doctoral thesis). University of Liege, Liege.
Quoilin, S., van den Broek UGent, M., Declaye, S., Dewallef, P., Lemort, V., 2014. Techno-economic survey of Organic Rankine Cycle (ORC) systems. Renewable & Sustainable Energy Reviews 22, 168–186.
Saitoh, T., Fujino, T., 2001. Advanced energy-efficient house (HARBEMAN house) with solar thermal, photovoltaic, and sky radiation energies (experimental results). Sol. Energy 70 (1), 63–77.
Saitoh, T., Yamada, N., Wakashima, S., 2007. Solar rankine cycle system using scroll expander. J. Environ. Eng. 2 (4), 2007.
Schimpf, S., Uitz, K., Span, R., 2011. Simulation of a solar assisted combined heat pump-organic Rankine cycle system. In: Proceedings of World Renewable Energy Congress 2011 Sweden.
Twomey, B., Jacobs, P.A., Gurgenci, H., 2013. Dynamic performance estimation of small-scale solar cogeneration with an organic Rankine cycle using a scroll expander. Appl. Therm. Eng. 51, 1307–1316.
Wang, X.D., Zhao, L., Wang, J.L., Zhang, W.Z., Zhao, X.Z., Wu, W., 2010. Performance evaluation of a low-temperature solar Rankine cycle using R245fa. Sol. Energy 84, 353–364.
Wolpert, J.L., Riffat, S.B., 1995. Solar-powered Rankine system for domestic application. Appl. Therm. Eng. 00032 (1), 1359–4311.
Yanagisawa, T., Cheng, M.C., Fukuta, M., Shimizu, T., 1990. Optimum operating pressure ratio for scroll compressor. In: Proceeding of the International Compressor Engineering Conference at Purdue, pp. 425–433.
Zanelli, R., Favrat, D., 1994. Experimental investigation of a hermetic scroll expander generator. In: International Compressor Engineering Conference, p. 1021.
Ziviani, D., Beyene, A., Venturini, M., 2014. Design, analysis and optimization of a micro-CHP system based on organic Rankine cycle system for ultralow grade thermal energy efficiency. J. Energy Resour. Technol. 136, 011602–011611.